

Supporting Information for

Energy Transfer from Multiple Excitons in a
Perovskite Nanocrystal to Organic Dyes
Revealed by Single-Particle Spectroscopy

Tetsuo Yamaguchi¹, Tomoya Fukumasu¹, Yukihide Ishibashi², and Sadahiro Masuo^{1}*

¹Department of Applied Chemistry for Environment, Kwansai Gakuin University, 1
Gakuen Uegahara, Sanda, Hyogo 669-1330, Japan

²Department of Applied Chemistry, Graduate School of Science and Engineering,
Ehime University, Matsuyama, Ehime 790-8577, Japan

Table of Contents

- 1. Absorption and PL spectra of PNCs dispersed in toluene**
- 2. Estimation of molar absorption coefficient of the PNC**
- 3. Estimation of Auger recombination rates**
- 4. Calculation of the energy transfer efficiency**
- 5. PL spectra of PNC–Cy3 systems dispersed in toluene**
- 6. Excitation spectra of PNC–Cy3 systems dispersed in toluene**
- 7. PL decay curves of PNC–Cy3 systems dispersed in toluene**
- 8. Transmission spectra of short-pass and long-pass filters**
- 9. Evaluation of emission photon statistics of the single pristine PNCs**
- 10. Confirmation of adsorption of multiple Cy3 dyes onto single PNCs**
- 11. Evaluation of ET from PNCs to Cy3 at the single PNC–Cy3 levels**
- 12. Evaluation of ET from MX in a single PNC to multiple Cy3 dyes**

1. Absorption and PL spectra of PNCs dispersed in toluene

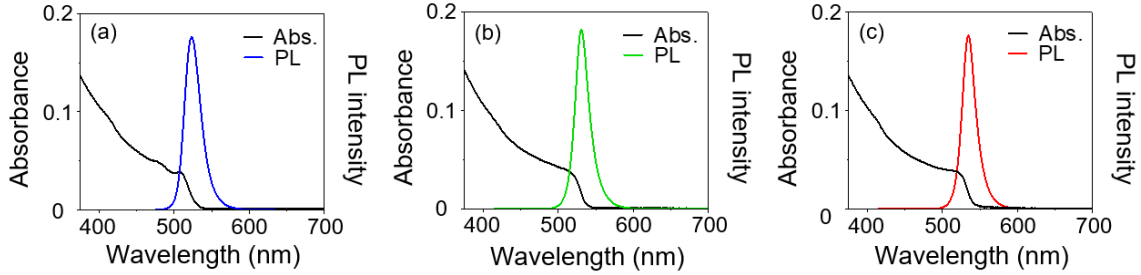


Figure S1. Absorption spectra (black lines) and PL spectra (colored lines) of **sPNC** (a), **mPNC** (b), and **lPNC** (c) dispersed in toluene. PL spectra were recorded under 442 nm excitation.

2. Estimation of molar absorption coefficient of the PNCs

The molar absorption coefficients (ε) of the PNCs were estimated based on a previous study, as follows. The absorption cross section (σ) of a FAPbBr₃ PNC with an edge length of 10.5 nm was reported to be $3.4 \times 10^{-14} \text{ cm}^2$.¹ The molar absorption coefficient for the PNC was calculated using equation S1:

$$\varepsilon = \sigma N_A / 2.303 \quad (\text{S1})$$

where N_A is Avogadro's number. The ε of PNCs has been reported to increase proportionally with the volume of the PNCs, as expressed by the following equation:²

$$\varepsilon = \frac{N_A \mu_i}{\ln 10} d^3 \quad (\text{S2})$$

where μ_i is the mean intrinsic absorption coefficient (cm^{-1}), and d is the edge length of the PNCs, respectively.

Based on the ε value of a PNC with an edge length of 10.5 nm ($= 8.9 \times 10^6 \text{ M}^{-1} \text{ cm}^{-1}$), the ε values for **sPNC**, **mPNC**, and **lPNC** were estimated to be $3.9 \times 10^6 \text{ M}^{-1} \text{ cm}^{-1}$, $1.3 \times 10^7 \text{ M}^{-1} \text{ cm}^{-1}$, and $3.1 \times 10^7 \text{ M}^{-1} \text{ cm}^{-1}$, respectively.

3. Estimation of Auger recombination rates

The Auger recombination (AR) rates of PNCs with different size distributions were evaluated by femtosecond transient absorption measurements. The transient absorption experiments were performed with a Ti: Sapphire regenerative amplifier system (Spectra-Physics, Tsunami and Spitfire ACE).³ The 400-nm pump pulse was generated by passing 50% of the fundamental light through a 1-mm BBO crystal. The other 800-nm light was guided into the collinear optical parametric amplifier system (Light Conversion, TOPAS-prime), and then a femtosecond 1340 nm light was generated. After passing through a controllable translational stage, which can generate an experimental delay time window of up to 1.5 ns between the pump and probe pulses, the 1340-nm light was then focused onto a 3-mm CaF₂ plate to create a supercontinuum light in the wavelength range of 400 nm to 940 nm, which served as the probe light. The intensity of the probe light was reduced to at least 1000 times lower than that of the pump light to avoid the excitation of the sample by the probe light. The probe light intensity passed through the sample was detected with a CCD camera (Bitran, BU-54DUV) combined with a polychromator (Chromex, 250is). The polarization of the pump beam was set to a magic angle (54.7°) with respect to that of the probe (NewFocus, Berek Polarization Compensator). The focusing pump beam diameter was 380 μm at the sample position, estimated from the laser beam pattern using thermal recording paper. The pump intensity varied in the range of 70 nJ cm⁻² pulse⁻¹ to 70 μJ cm⁻² pulse⁻¹ (130 fs FWHM) by adjusting the variable neutral density filter. The sample was placed in a home-built rotation cell with a 2 mm optical path length to minimize photodegradation. It was noted that the laser-induced decomposition of the sample was not observed, even at a high laser fluence of 70 μJ cm⁻² pulse⁻¹, because we confirmed that the steady-state absorption spectra remained

unchanged before and after the measurement. Data were analyzed using Igor (WaveMetrics) and homemade programs. The number of excitons generated per excitation pulse $\langle N \rangle$ was estimated from the pump intensity and absorption cross sections of the PNCs (**sPNC**: $2.3 \times 10^{-14} \text{ cm}^2$, **mPNC**: $9.8 \times 10^{-14} \text{ cm}^2$, and **L PNC**: $1.8 \times 10^{-13} \text{ cm}^2$).

As a representative example, transient absorption spectra of **sPNC** excited by $70 \text{ } \mu\text{J cm}^{-2} \text{ pulse}^{-1}$ are shown in Figure S2, where $\langle N \rangle = 8.6$.

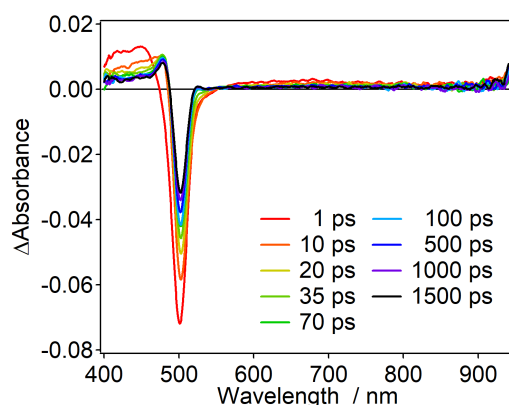


Figure S2. Transient absorption spectra of **sPNC** in toluene excited at 400 nm with $185 \text{ } \mu\text{J cm}^{-2} \text{ pulse}^{-1}$ ($\langle N \rangle = 8.6$).

Bleach recovery observed in the transient absorption spectra was plotted to estimate the lifetimes of Auger recombination, i.e., lifetimes of multiple excitons, as shown in Figure S3. The $\Delta\text{Absorbance}$ at 505 nm for **sPNC**, 524 nm for **mPNC**, and 528 nm for **L PNC** was plotted. The excitation intensities varied in $3.6\text{-}185 \text{ } \mu\text{J cm}^{-2} \text{ pulse}^{-1}$ for **sPNC**, $1.1\text{-}370 \text{ } \mu\text{J cm}^{-2} \text{ pulse}^{-1}$ for **mPNC**, and $0.49\text{-}156 \text{ } \mu\text{J cm}^{-2} \text{ pulse}^{-1}$ for **L PNC**, which corresponded to $\langle N \rangle = 0.17\text{-}8.6$ for **sPNC**, $\langle N \rangle = 0.23\text{-}73$ for **mPNC**, and $\langle N \rangle = 0.18\text{-}58$ for **L PNC**. In the three PNCs, a short lifetime component was observed at higher $\langle N \rangle$.

The contribution of the short lifetime components, attributable to AR, appeared at $\langle N \rangle > 1$ and increased with increase of $\langle N \rangle$. When compared with similar $\langle N \rangle$, the contribution of AR was lower in larger PNCs. As an example, Figure S4 shows bleach recovery kinetics with $\langle N \rangle \approx 2$ of the three PNCs. The contribution of AR was remarkably higher in **sPNC** compared to the other two. At higher $\langle N \rangle$, short lifetime components were clearly observed in **mPNC** and **L PNC**, and the AR lifetimes of **sPNC**, **mPNC**, and **L PNC** were estimated to be 40 ps, 100 ps, and 300 ps, respectively. It indicates that the AR efficiency was lower in larger PNCs due to the absence of quantum confinement effect in the PNCs, that is, the long exciton-exciton distance leads to low efficiency and results in slow AR. This suggests that, in larger PNCs, a greater number of excitons can be recombined radiatively without undergoing AR. This is consistent with the results obtained from photon correlation measurements of single PNCs. It was noteworthy that the additional short lifetime component of 20 ps was observed when $\langle N \rangle > 4$ in **mPNC** and $\langle N \rangle > 14$ in **L PNC**. This component is attributed to AR of excitons generated in short distance due to high population of excitons in a PNC.

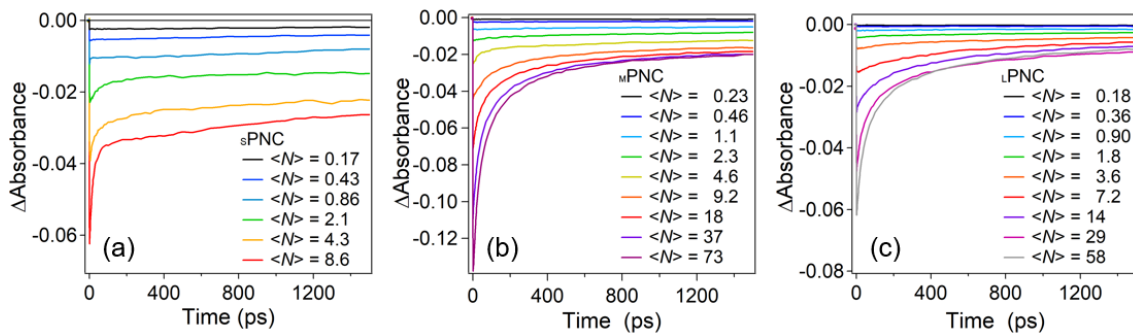


Figure S3. Bleach recovery kinetics of **sPNC** (a), **mPNC** (b), and **L PNC** (c) excited by 400 nm laser with intensities to generate several $\langle N \rangle$. The kinetics were measured at 505 nm for **sPNC**, 524 nm for **mPNC**, and 528 nm for **L PNC**.

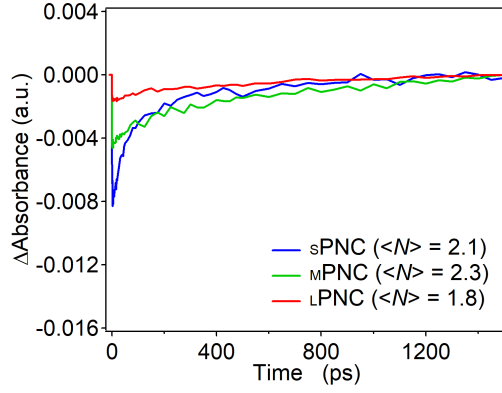


Figure S4. Bleach recovery kinetics with $\langle N \rangle \approx 2$ in **sPNC** (blue line), **mPNC** (green line), and **lPNC** (red line).

4. Calculation of the energy transfer efficiency

The Förster radius (R_0) for the energy transfer between FAPbBr₃ PNC donors and Cy3 acceptors was calculated using Equation S3

$$R_0 = 0.211 \times \left(\frac{\Phi_D \kappa^2}{n^4} J(\lambda) \right)^{\frac{1}{6}} \quad (\text{S3})$$

where Φ_D is the PLQY of the PNCs in the absence of the acceptor, n is the refractive index of the medium, and κ^2 is the orientation factor, which depends on the relative orientation of the donor and acceptor dipoles. A value of $\kappa^2 = 0.476$ was used, assuming isotropic transition dipoles in the PNCs and Cy3 molecules fixed on the PNC surface.⁴

$J(\lambda)$ is the spectral overlap integral, expressed by Equation S4:

$$J(\lambda) = \int_0^\infty F_D(\lambda) \varepsilon_A(\lambda) \lambda^4 d\lambda \quad (\text{S4})$$

where $F_D(\lambda)$ is the normalized PL intensity of the PNC in the wavelength range $\lambda - \lambda +$

($\Delta \lambda$), with the total intensity normalized to unity. $\varepsilon_A(\lambda)$ is the extinction coefficient of the acceptor at λ . $J(\lambda) = 6.32 \times 10^{15}$ for **sPNC-Cy3**, 7.66×10^{15} for **mPNC-Cy3**, and $8.14 \times 10^{15} \text{ nm}^4\text{M}^{-1}\text{cm}^{-1}$ for **LPNC-Cy3** was estimated from the overlap between PL spectra of the PNCs and absorption spectrum of Cy3. By substituting the $J(\lambda)$ values ($\Phi_D = 81\%$ for **sPNC-Cy3**, 82% for **mPNC-Cy3**, and 68% for **LPNC-Cy3**), $\kappa^2 = 0.476$, and $n = 1.496$ into Equation S3, the R_0 values of 5.9 nm for **sPNC-Cy3**, 6.1 nm for **mPNC-Cy3** and 6.0 nm for **LPNC-Cy3** are obtained. The theoretical energy transfer efficiency (E_{FRET}) was then calculated by Equation S5:

$$E_{\text{FRET}} = \frac{NR_0^6}{NR_0^6 + r^6} \quad (\text{S5})$$

where r is the distance between the donor and acceptor, and N is the number of Cy3 molecules adsorbed onto a single PNC. The r values have distribution from the shortest (between the center of the PNC and the center of a Cy3 molecule adsorbed through a carboxy group) to the longest (between the edge of the PNC and the center of a Cy3 molecule), so that the shortest r values were 4.9 nm for **sPNC-Cy3**, 6.8 nm for **mPNC-Cy3**, and 8.9 nm for **LPNC-Cy3** and longest r values were 7.8 nm for **sPNC-Cy3**, 8.9 nm for **mPNC-Cy3**, and 14.7 nm for **LPNC-Cy3**. By substituting r and R_0 into Equation S5, the theoretical E_{FRET} values were obtained and shown as vertical lines in Figure 4 of the main text and Figure S6.

The experimental energy transfer efficiencies (E_{ET}) were estimated from PL quenching of the PNCs using Equation S6:

$$E_{\text{ET}} = \frac{I_0 - I}{I_0} \times 100 \quad (\text{S6})$$

where, I_0 and I are the PL intensities of the PNCs in the absence and presence of Cy3, respectively.

5. PL spectra of PNC-Cy3 systems dispersed in toluene

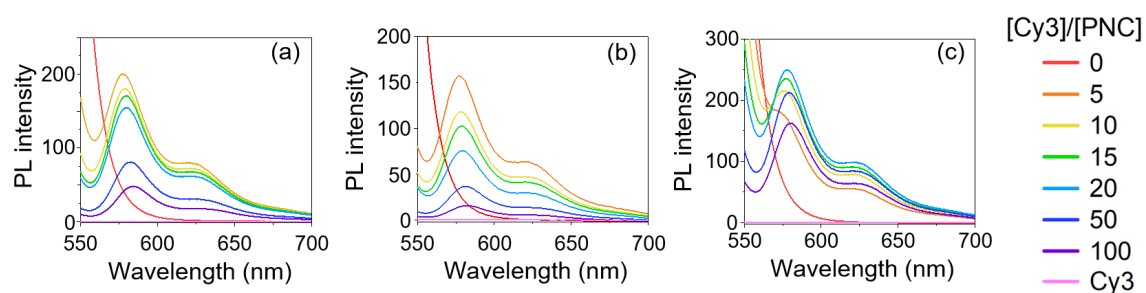


Figure S5. PL spectra of s PNC-Cy3 (a), m PNC-Cy3 (b), and l PNC-Cy3 (c) in toluene with varying $[Cy3]/[PNC]$ ratios, recorded under 405 nm. For comparison, the PL spectrum of pristine Cy3 in toluene at 2.5×10^{-7} M is also shown in each panel (pink lines).

6. Excitation spectra of PNC-Cy3 systems dispersed in toluene

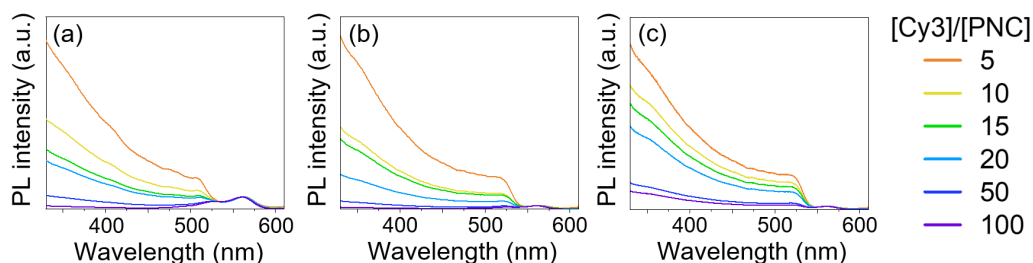


Figure S6. Excitation spectra of **sPNC-Cy3** (a), **mPNC-Cy3** (b), and **lPNC-Cy3** (c) dispersed in toluene, recorded by monitoring PL intensity at 620 nm. All spectra are normalized at 562 nm.

7. PL decay curves of PNC-Cy3 systems dispersed in toluene

PL decay curves were measured using a set up comprising a Ti:Sapphire laser (80 MHz, 100 fs full width at half-maximum, Mai-tai, Spectra-Physics) and an avalanche photodiode (APD, PD-050-CTD, MPD). The 920 nm fundamental laser was tuned to 460 nm and 1 MHz by a frequency doubler/pulse selector (Model 3980, Spectra-Physics). The PL was detected by the APD via a monochromator (M10, Jasco). The signals from the APD were connected to a picosecond histogram ambulating real-time processor (HydraHarp 400, PicoQuant) to measure the PL lifetimes. The time-resolution of the lifetime measurement, i.e., the instrumental response function (IRF) of the system, was estimated to be 20 ps. The PL decay curves of **sPNC**, **mPNC**, **lPNC**, and **Cy3** in the **PNC-Cy3** systems were recorded by detecting at 524, 530, 535, and 620 nm, respectively, using 460 nm excitation. As shown in Figure S7, the PL decay curves of the PNCs became shorter with the increasing $[\text{Cy3}]/[\text{PNCs}]$ ratio. This shortening indicates ET from the PNCs to Cy3 to give ET lifetimes of 0.79 ns for **sPNC-Cy3**, 1.7 ns for **mPNC-Cy3** and

2.2 ns for **L**PNC-Cy3 at $[\text{Cy3}]/[\text{PNC}] = 10$. In the PL decay curves detected of Cy3 (Figure S8), rise components slower than the IRF were observed in the three PNC-Cy3 systems and the rise components were consistent with the ET lifetimes. These results suggest that the ET rate in larger PNCs slowed down due to the longer PNC-Cy3 distance, which agrees with the size-dependent E_{ET} trend observed in the PL quenching measurements (Figure 3 in the main text).

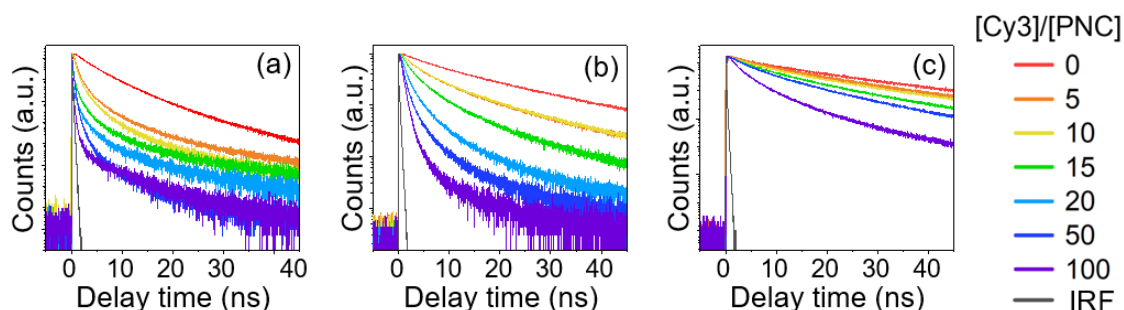


Figure S7. PL decay curves of PNCs in **s**PNC-Cy3 (a), **m**PNC-Cy3 (b), and **l**PNC-Cy3 (c) dispersed in toluene at various $[\text{Cy3}]/[\text{PNCs}]$ ratios, with the instrument response function (IRF; black lines). Excitation wavelength: 460 nm.

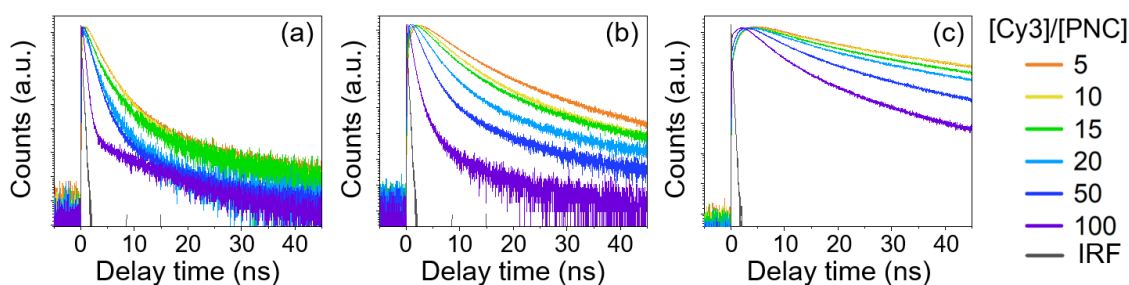


Figure S8. PL decay curves of Cy3 in **s**PNC-Cy3 (a), **m**PNC-Cy3 (b), and **l**PNC-Cy3 (c) dispersed in toluene at various $[\text{Cy3}]/[\text{PNCs}]$ ratios, with IRF (black lines). Excitation wavelength: 460 nm.

E_{ET} was also estimated from the PL lifetimes of the PNCs using Equation S7:

$$E_{ET} = \frac{\tau_{ave0} - \tau_{ave}}{\tau_{ave0}} \times 100 \quad (S7)$$

where τ_{ave0} and τ_{ave} are the averaged PL lifetimes of the PNCs in the absence and presence of Cy3, respectively. The estimated E_{ET} values are compared to the theoretical E_{FRET} estimated with the shortest and longest PNC-Cy3 distances in Figure S9. The agreement between E_{ET} and E_{FRET} supports the conclusion that ET from the PNCs to Cy3 proceeds via the FRET mechanism.

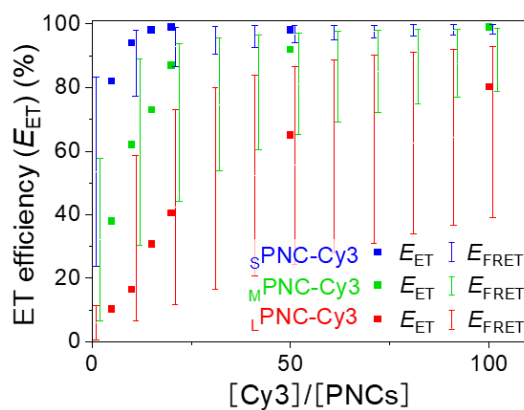


Figure S9. Energy transfer efficiencies (E_{ET}) estimated from PL lifetime shortening of the PNCs in the **PNC-Cy3** systems (dots), compared with E_{FRET} (solid lines) estimated from FRET theory.

8. Transmission spectra of short-pass and long-pass filters

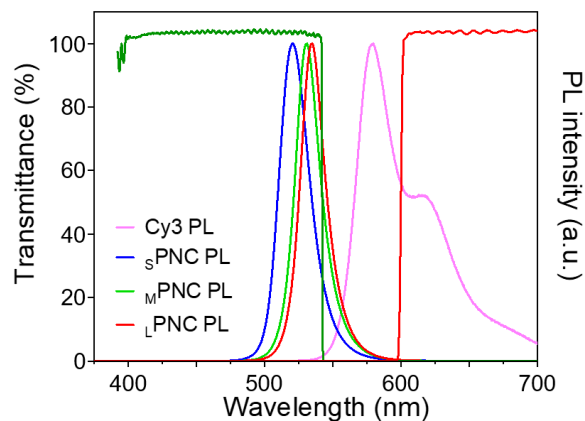


Figure S10. Transmission spectra of a SP filter (dark green line) and an LP filter (red line), overlaid with the PL spectra of Cy3 (pink line) and the PNCs (blue, green, and red lines).

9. Evaluation of emission photon statistics of single pristine PNCs

The emission photon statistics from single pristine PNCs were observed under 442 nm excitation. As shown in Figure S11, the AFM topography image (a) and PL image (b) of single PNCs in the same area were obtained by scanning the sample. Time traces of PL intensity, PL spectra, and photon correlation histograms for single PNCs were subsequently measured. Representative results from individual s PNC, m PNC, and l PNC are shown in Figures S12-S20.

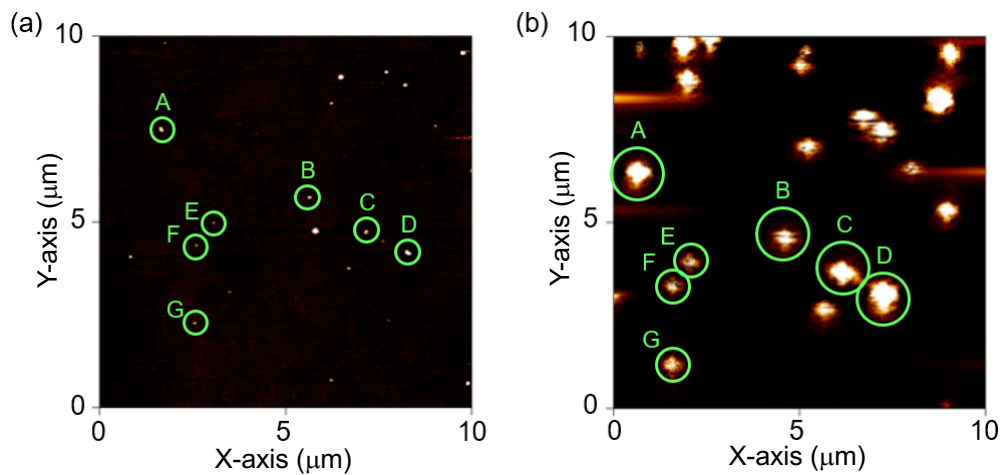


Figure S11. AFM topography (a) and PL images (b) of single $mPNCs$ at the same area on a coverslip.

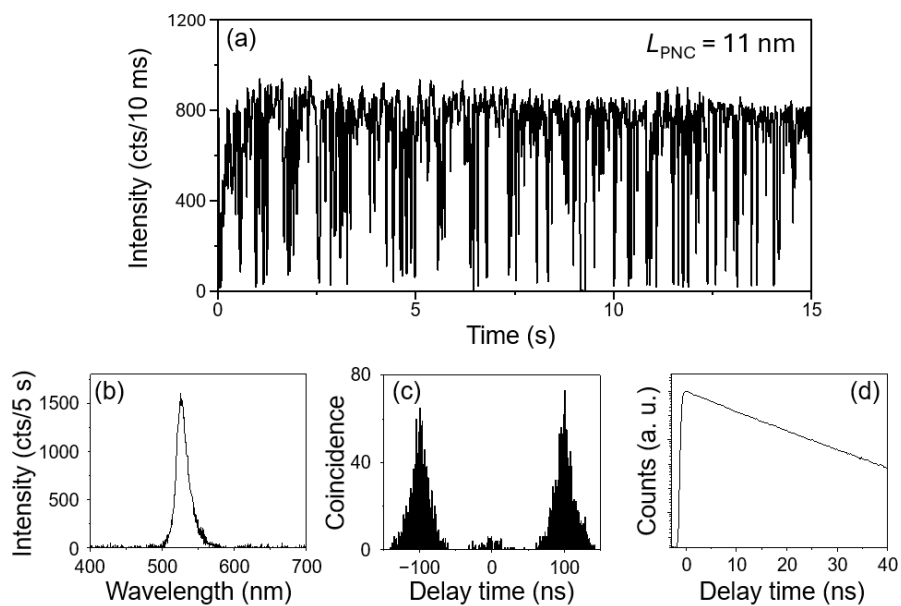


Figure S12. Time trace of PL intensity (a), PL spectrum (b), photon correlation histogram (c), and PL decay curve (d) detected from a single PNC with $L_{PNC} = 11$ nm under 442 nm excitation.

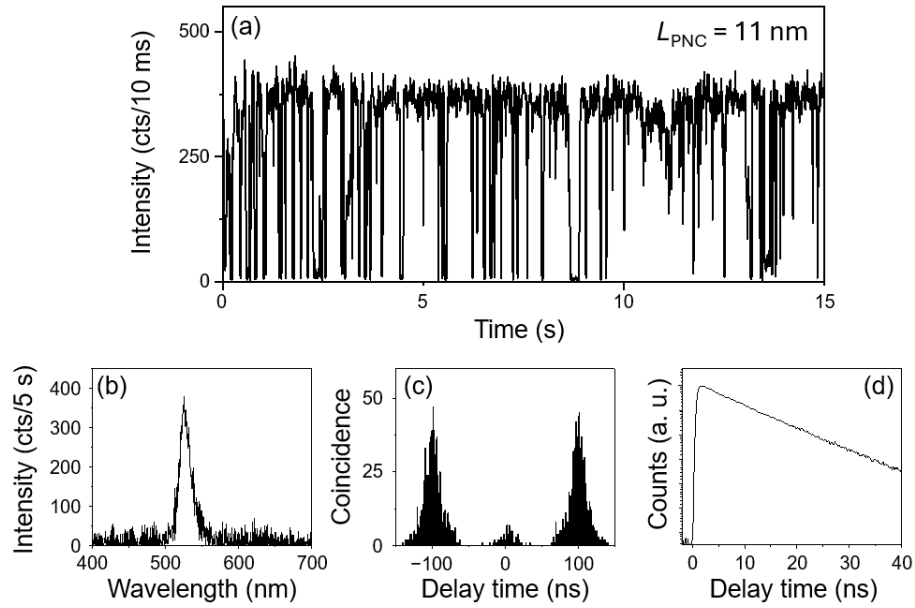


Figure S113. Time trace of PL intensity (a), PL spectrum (b), photon correlation histogram (c), and PL decay curve (d) detected from a single PNC with $L_{\text{PNC}} = 11 \text{ nm}$ under 442 nm excitation.

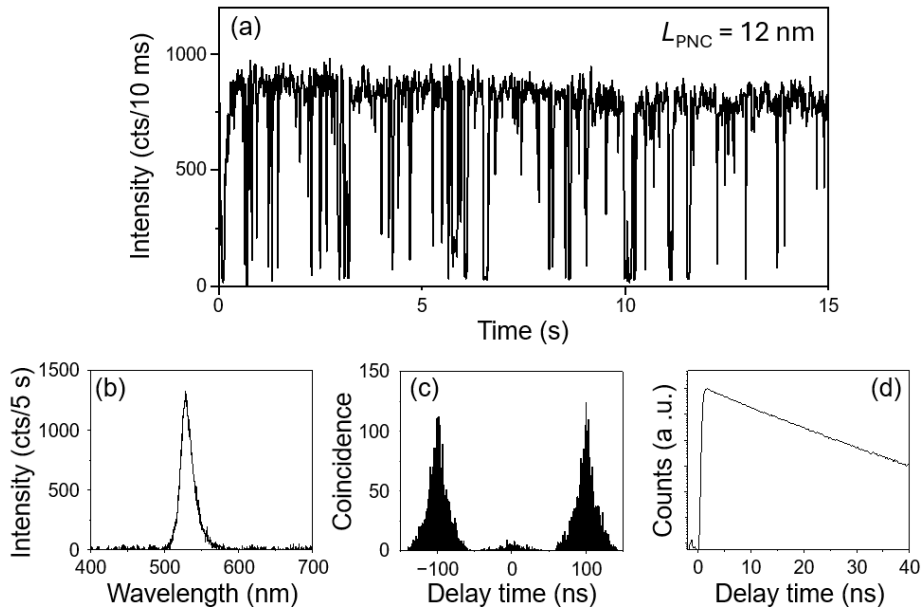


Figure S114. Time trace of PL intensity (a), PL spectrum (b), photon correlation histogram (c), and PL decay curve (d) detected from a single PNC with $L_{\text{PNC}} = 12 \text{ nm}$ under 442 nm excitation.

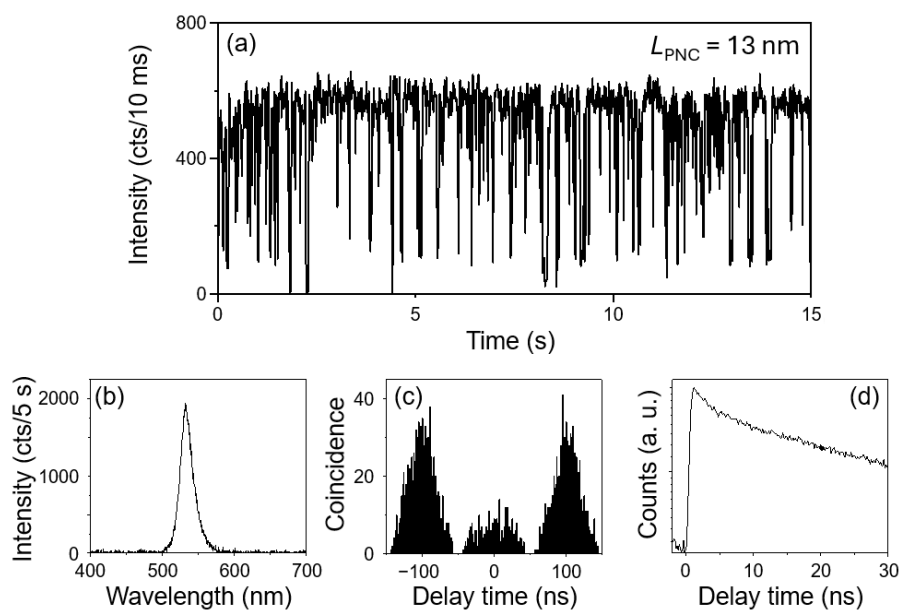


Figure S115. Time trace of PL intensity (a), PL spectrum (b), photon correlation histogram (c), and PL decay curve (d) detected from a single PNC with $L_{\text{PNC}} = 13 \text{ nm}$ under 442 nm excitation.

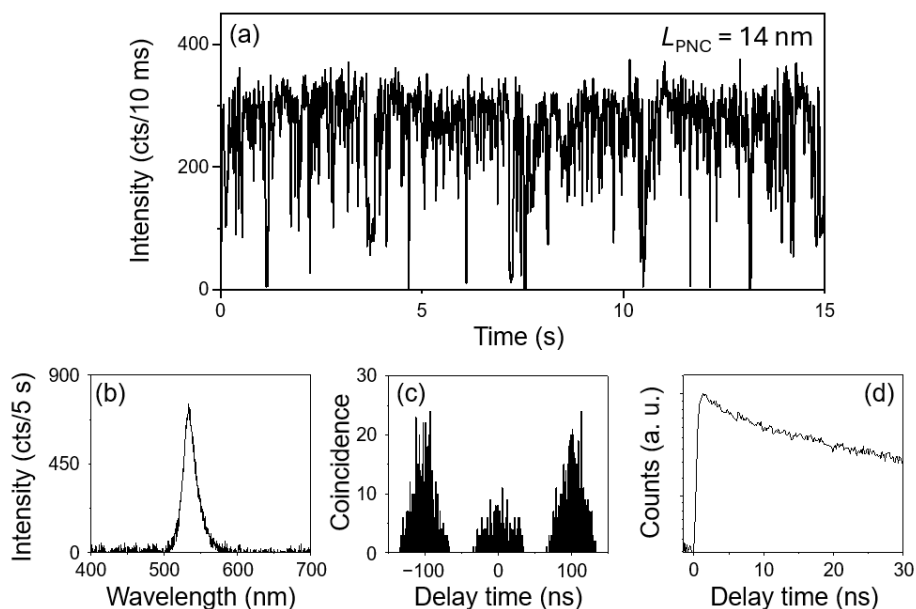


Figure S116. Time trace of PL intensity (a), PL spectrum (b), photon correlation histogram (c), and PL decay curve (d) detected from a single PNC with $L_{\text{PNC}} = 14 \text{ nm}$ under 442 nm excitation.

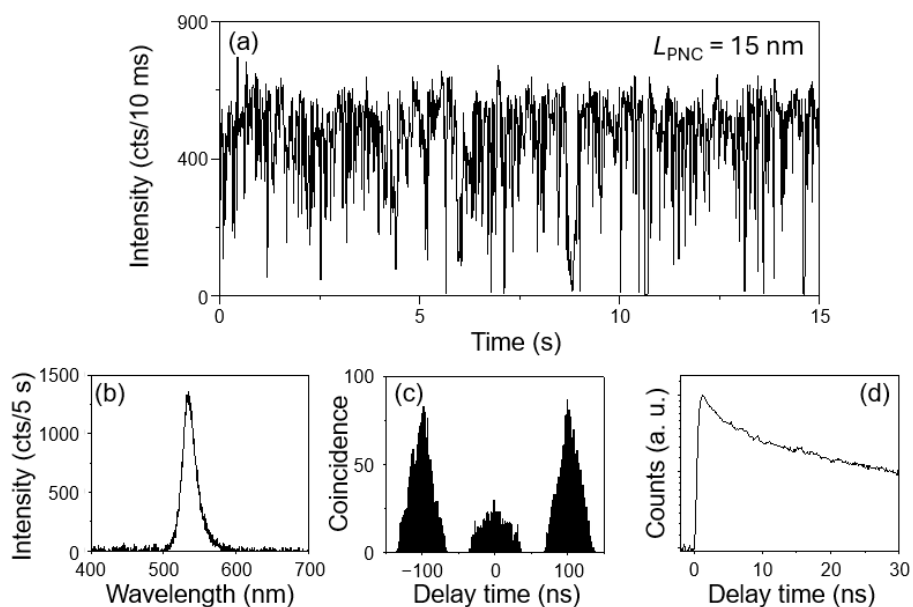


Figure S17. Time trace of PL intensity (a), PL spectrum (b), photon correlation histogram (c), and PL decay curve (d) detected from a single PNC with $L_{\text{PNC}} = 15 \text{ nm}$ under 442 nm excitation.

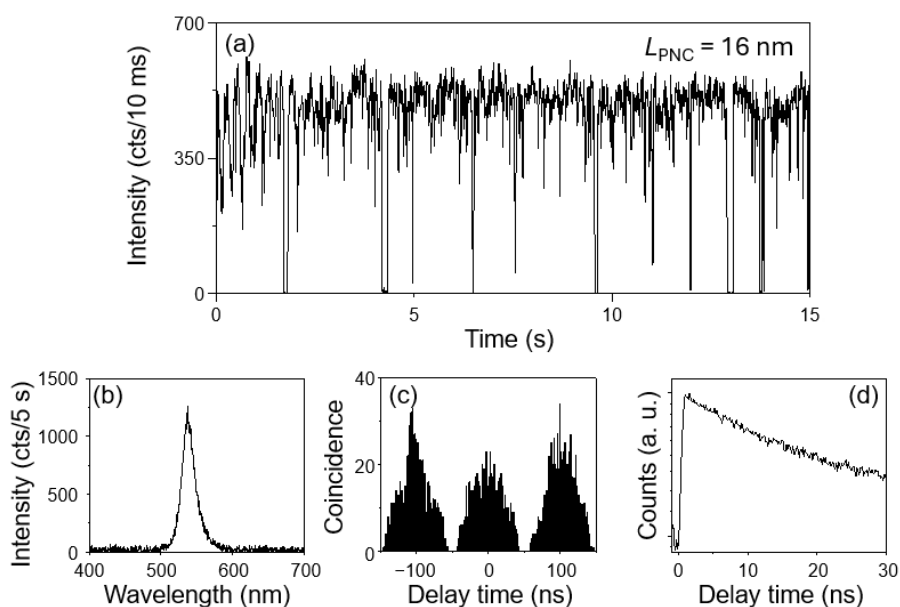


Figure S18. Time trace of PL intensity (a), PL spectrum (b), photon correlation histogram (c), and PL decay curve (d) detected from a single PNC with $L_{\text{PNC}} = 16 \text{ nm}$ under 442 nm excitation.

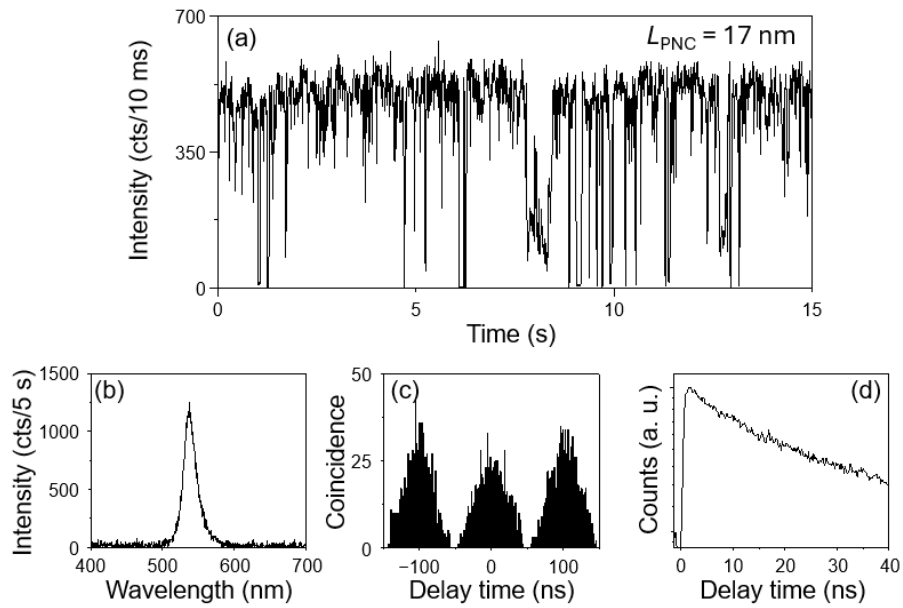


Figure S19. Time trace of PL intensity (a), PL spectrum (b), photon correlation histogram (c), and PL decay curve (d) detected from a single PNC with $L_{\text{PNC}} = 17 \text{ nm}$ under 442 nm excitation.

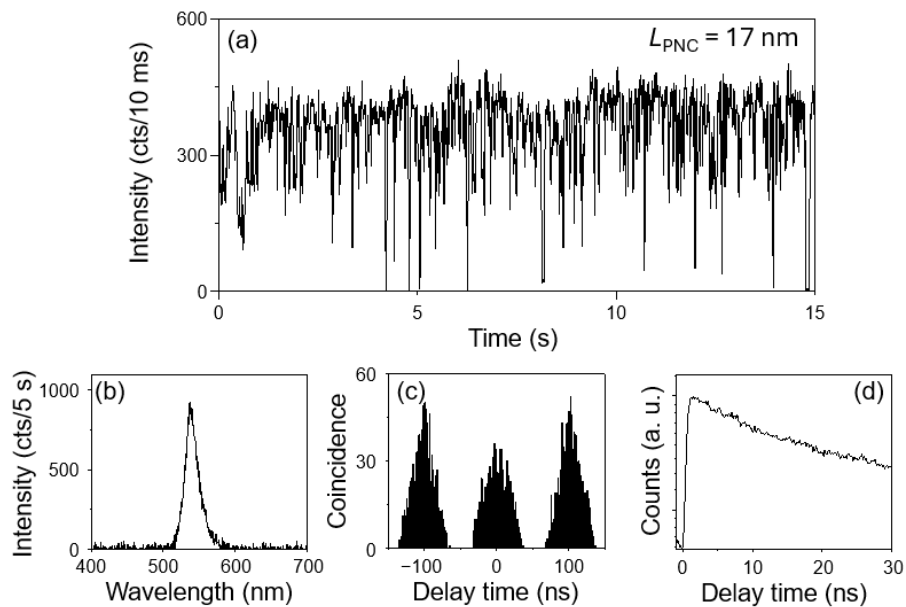


Figure S20. Time trace of PL intensity (a), PL spectrum (b), photon correlation histogram (c), and PL decay curve (d) detected from a single PNC with $L_{\text{PNC}} = 17 \text{ nm}$ under 442 nm excitation.

10. Confirmation of adsorption of multiple Cy3 dyes onto single PNCs

To verify the adsorption of multiple Cy3 dye molecules onto individual PNCs, photon correlation measurements were conducted by selectively exciting Cy3 with a 532 nm laser beam. Time traces of PL intensity, PL spectra, and photon correlation histograms for representative individual **sPNC-Cy3**, **mPNC-Cy3**, and **lPNC-Cy3** systems are presented in Figures S21-S29.

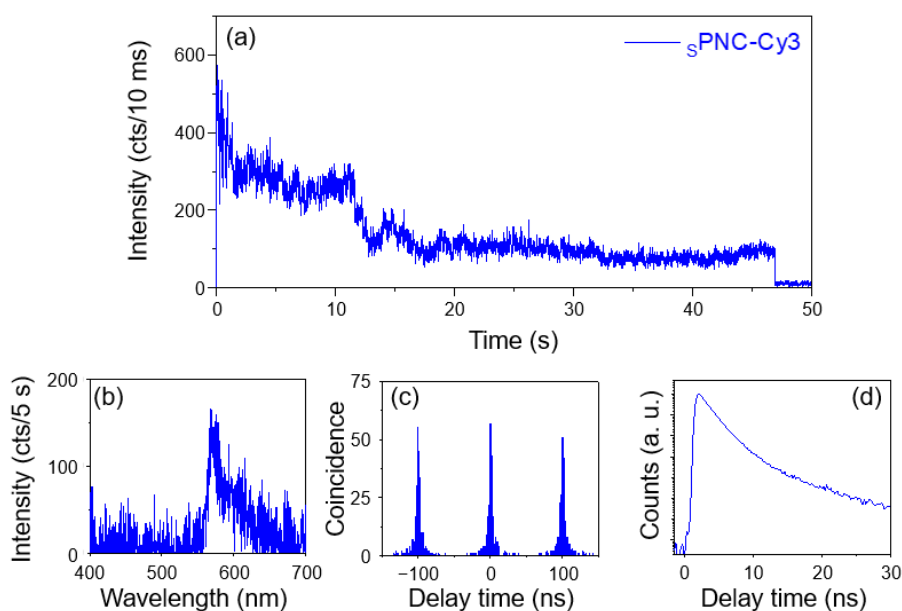


Figure S21. Time trace of PL intensity (a), PL spectrum (b), photon correlation histogram (c), and PL decay curve (d) detected from Cy3 in a single **sPNC-Cy3** system upon excitation with a 532 nm laser.

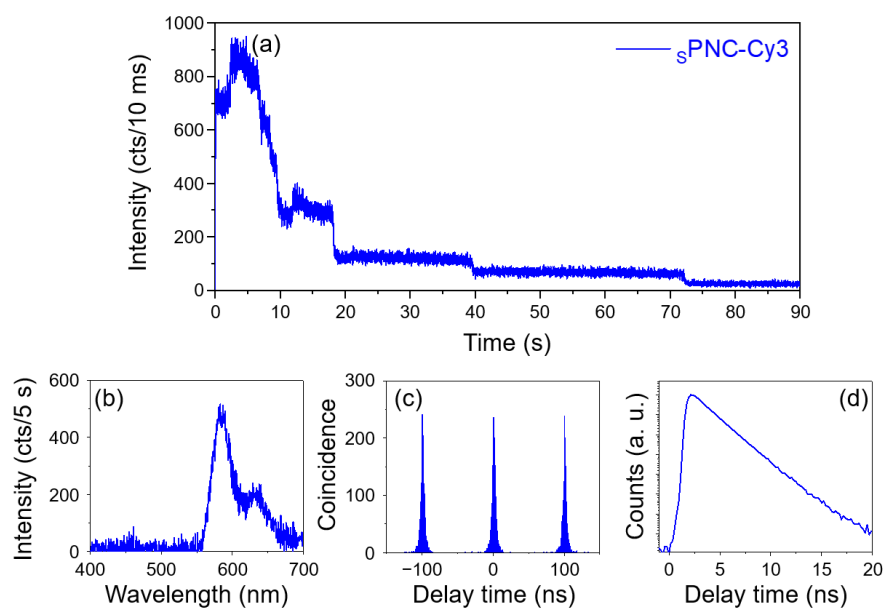


Figure S22. Time trace of PL intensity (a), PL spectrum (b), photon correlation histogram (c), and PL decay curve (d) detected from Cy3 in a single sPNC-Cy3 system upon excitation with a 532 nm laser.

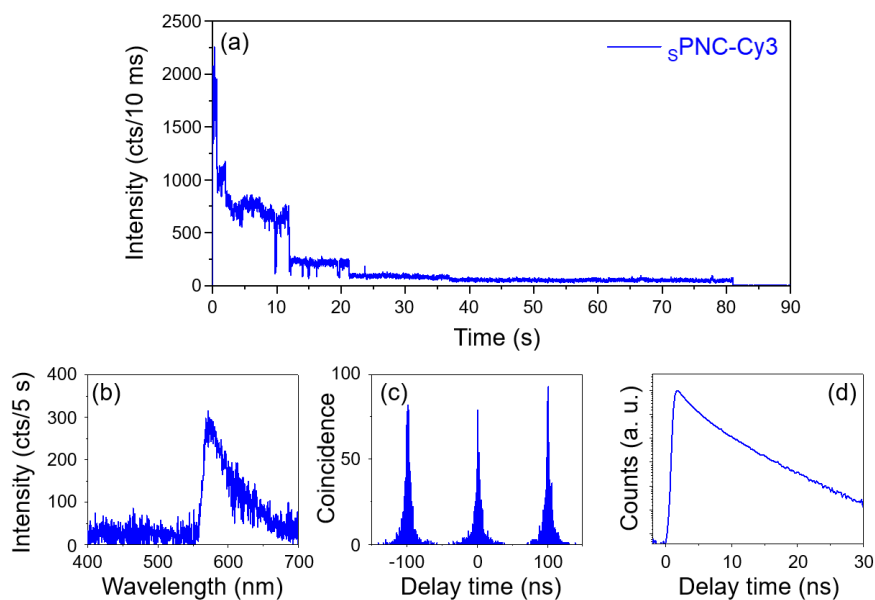


Figure S23. Time trace of PL intensity (a), PL spectrum (b), photon correlation histogram (c), and PL decay curve (d) detected from Cy3 in a single sPNC-Cy3 system upon excitation with a 532 nm laser.

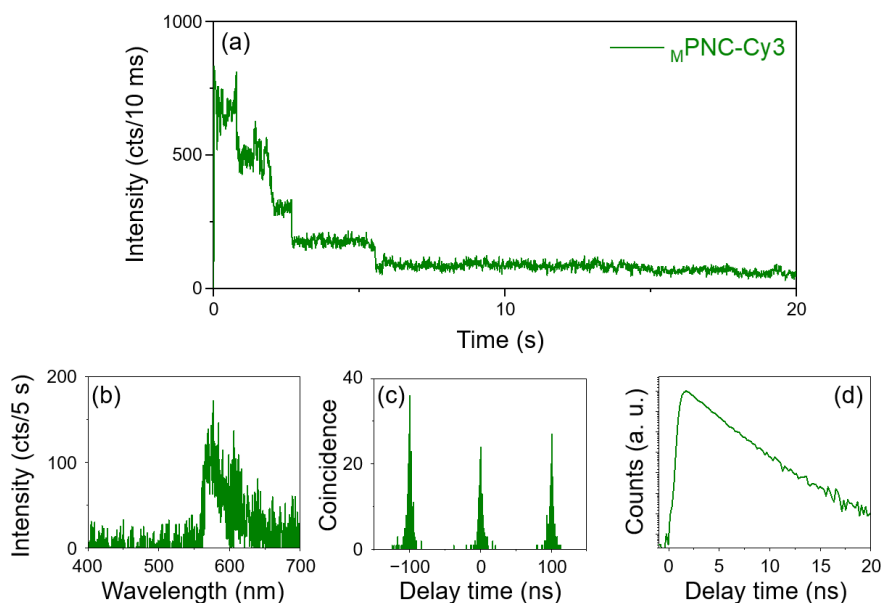


Figure S24. Time trace of PL intensity (a), PL spectrum (b), photon correlation histogram (c), and PL decay curve (d) detected from Cy3 in a single $mPNC-Cy3$ system upon excitation with a 532 nm laser.

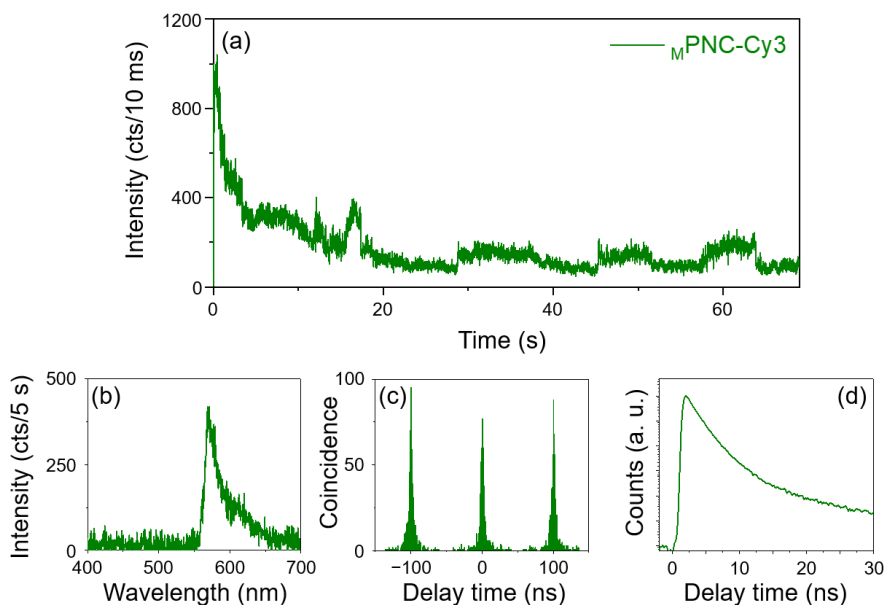


Figure S25. Time trace of PL intensity (a), PL spectrum (b), photon correlation histogram (c), and PL decay curve (d) detected from Cy3 in a single $mPNC-Cy3$ system upon excitation with a 532 nm laser.

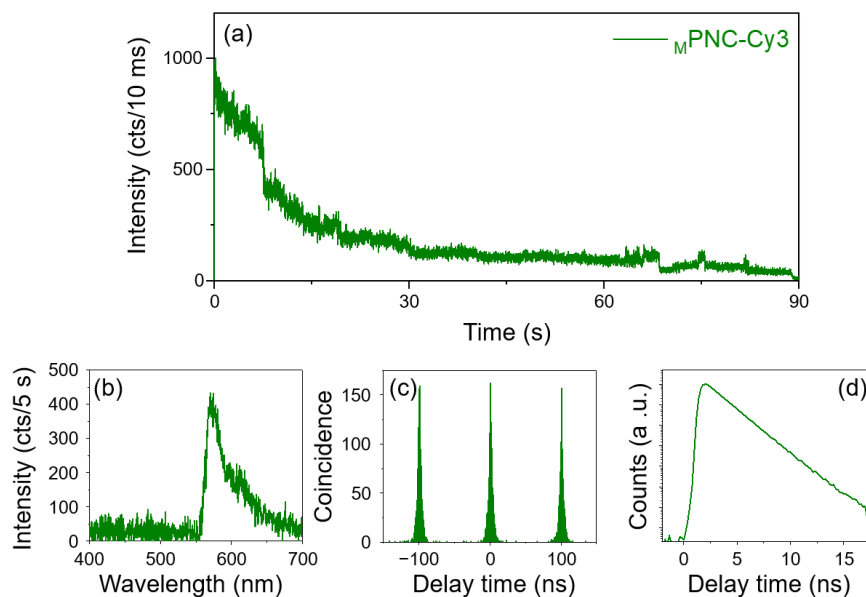


Figure S26. Time trace of PL intensity (a), PL spectrum (b), photon correlation histogram (c), and PL decay curve (d) detected from Cy3 in a single $mPNC-Cy3$ system upon excitation with a 532 nm laser.

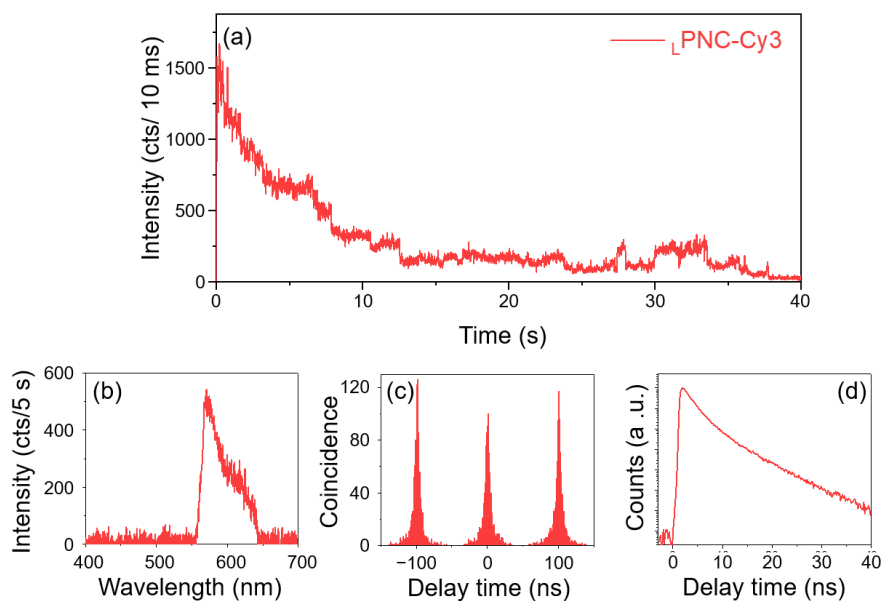


Figure S27. Time trace of PL intensity (a), PL spectrum (b), photon correlation histogram (c), and PL decay curve (d) detected from Cy3 in a single $lPNC-Cy3$ system upon excitation with a 532 nm laser.

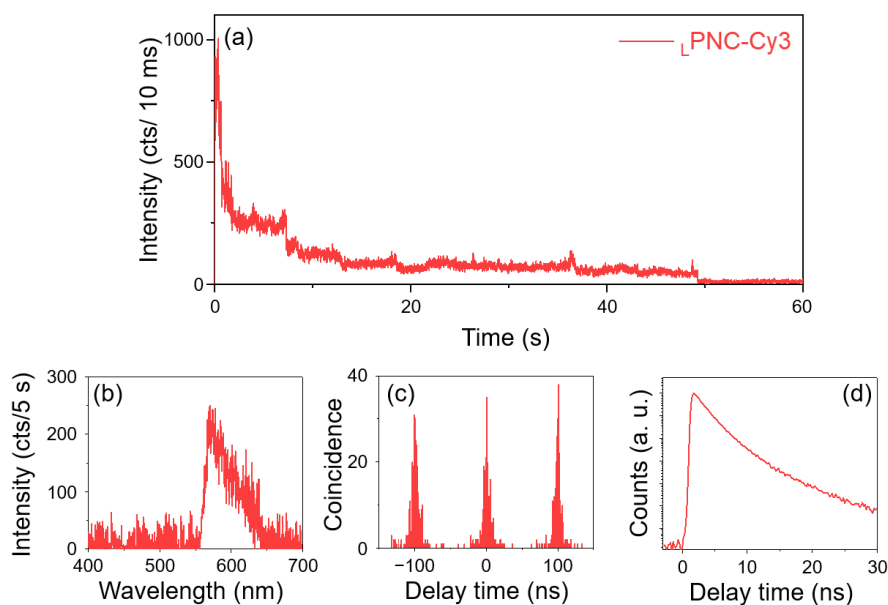


Figure S28. Time trace of PL intensity (a), PL spectrum (b), photon correlation histogram (c), and PL decay curve (d) detected from Cy3 in a single $L_{\text{PNC-Cy3}}$ system upon excitation with a 532 nm laser.

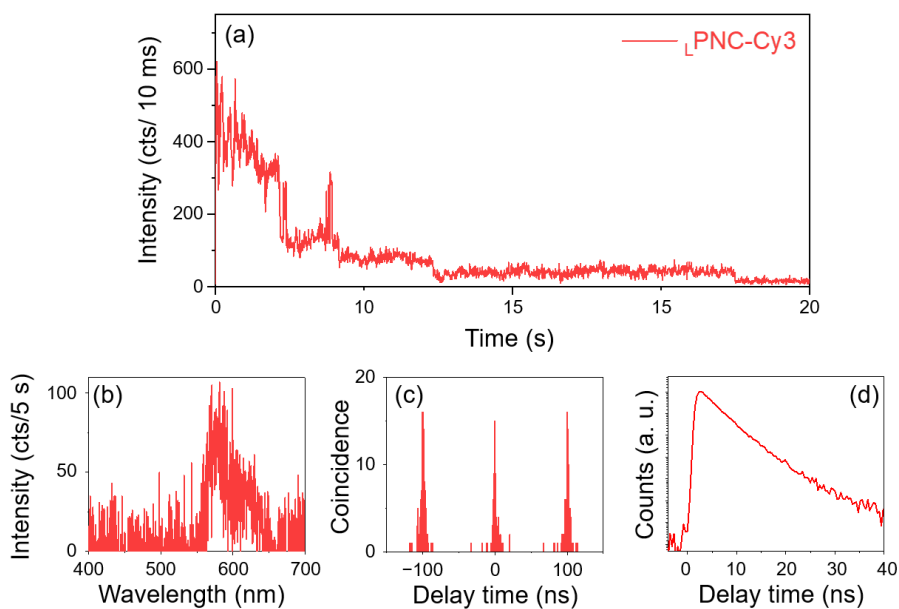


Figure S29. Time trace of PL intensity (a), PL spectrum (b), photon correlation histogram (c), and PL decay curve (d) detected from Cy3 in a single $L_{\text{PNC-Cy3}}$ system upon excitation with a 532 nm laser.

11. Evaluation of ET from PNCs to Cy3 at the single PNC-Cy3 level

The ET from PNCs to adsorbed Cy3 at the single **PNC-Cy3** level was monitored by selectively exciting the PNCs at 442 nm. PL from the PNCs and Cy3 was detected simultaneously using two APDs with SP and LP filters. Initially, PL images of the same area were captured with and without the LP filter, as shown in Figure S30. In the images, PL from the PNCs and Cy3 were detected without the LP filter, whereas only the PL from Cy3 was detected with the LP filter. The consistent positions of the PL spots in the images suggested that the PNCs and Cy3 co-existed, and ET from the PNCs to Cy3 occurred at the single PNC level. By selecting individual PL spots, time traces of PL intensity, PL spectra, and PL decay curves were measured from the single PNC-Cy3 to evaluate the ET from the PNCs to the adsorbed Cy3. Representative results from individual **sPNC-Cy3**, **mPNC-Cy3**, and **LPNC-Cy3** systems are shown in Figure S31-38.

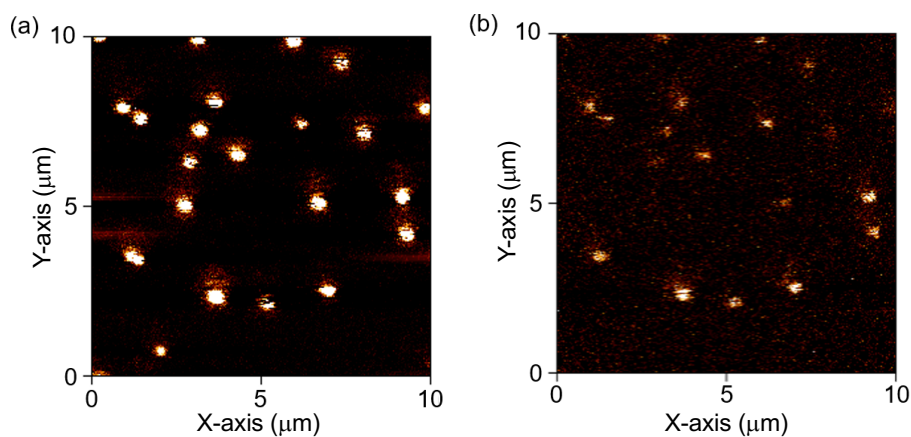


Figure S30. PL images of a single **mPNC-Cy3** dispersed in a PMMA thin film under 442 nm excitation. (a) PL from the PNC and Cy3 were detected without the LP filter. (b) Only PL from the Cy3 was detected with the LP filter.

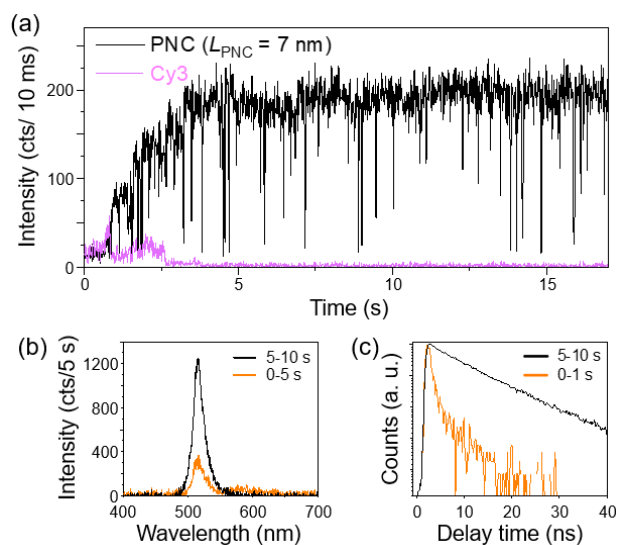


Figure S31. (a) Time traces of PL intensity detected from Cy3 (pink line) and the PNC (black line) in a single **PNC-Cy3** system under 442 nm excitation. (b) PL spectra collected from the single **PNC-Cy3** system during 0–5 s (orange line) and 10–15 s (black line) in the time trace shown in (a). The PNC size was estimated to be $L_{\text{PNC}} = 7$ nm based on the PL peak. (c) PL decay curves of the PNC detected during 0–1 s (orange line) and 5–10 s (black line) in the time trace shown in (a).

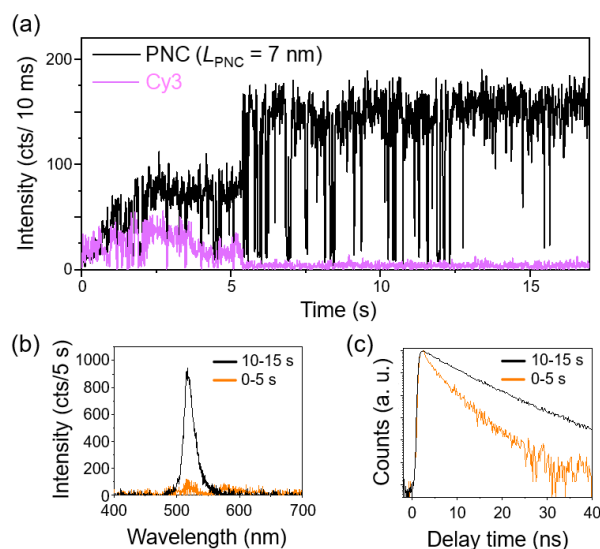


Figure S32 (a) Time traces of PL intensity detected from Cy3 (pink line) and the PNC (black line) in a single **PNC-Cy3** system under 442 nm excitation. (b) PL spectra collected from the single **PNC-Cy3** system during 0–5 s (orange line) and 10–15 s (black line) in the time trace shown in (a). The PNC size was estimated to be $L_{\text{PNC}} = 7$ nm based on the PL peak. (c) PL decay curves of the PNC detected during 0–5 s (orange line) and 10–15 s (black line) in the time trace shown in (a).

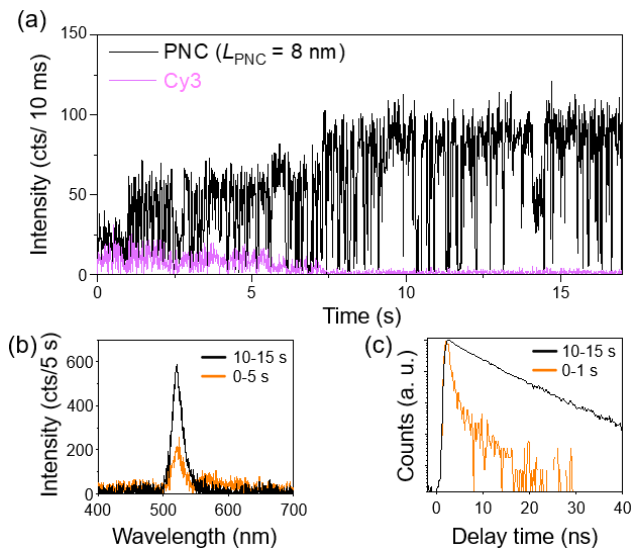


Figure S33. (a) Time traces of PL intensity detected from Cy3 (pink line) and the PNC (black line) in a single **PNC-Cy3** system under 442 nm excitation. (b) PL spectra collected from the single **PNC-Cy3** system during 0–5 s (orange line) and 10–15 s (black line) in the time trace shown in (a). The PNC size was estimated to be $L_{\text{PNC}} = 8 \text{ nm}$ based on the PL peak. (c) PL decay curves of the PNC detected during 0–1 s (orange line) and 10–15 s (black line) in the time trace shown in (a).

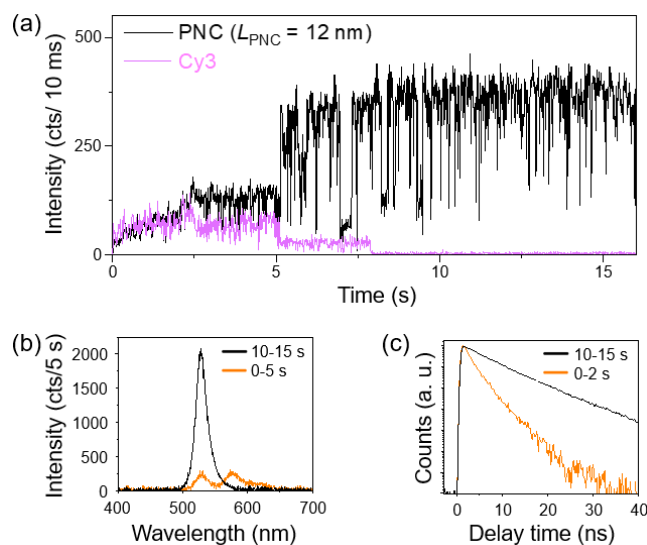


Figure S34. (a) Time traces of PL intensity detected from Cy3 (pink line) and the PNC (black line) in a single **PNC-Cy3** system under 442 nm excitation. (b) PL spectra collected from the single **PNC-Cy3** system during 0–5 s (orange line) and 10–15 s (black line) in the time trace shown in (a). The PNC size was estimated to be $L_{\text{PNC}} = 12 \text{ nm}$ based on the PL peak. (c) PL decay curves of the PNC detected during 0–2 s (orange line) and 10–15 s (black line) in the time trace shown in (a).

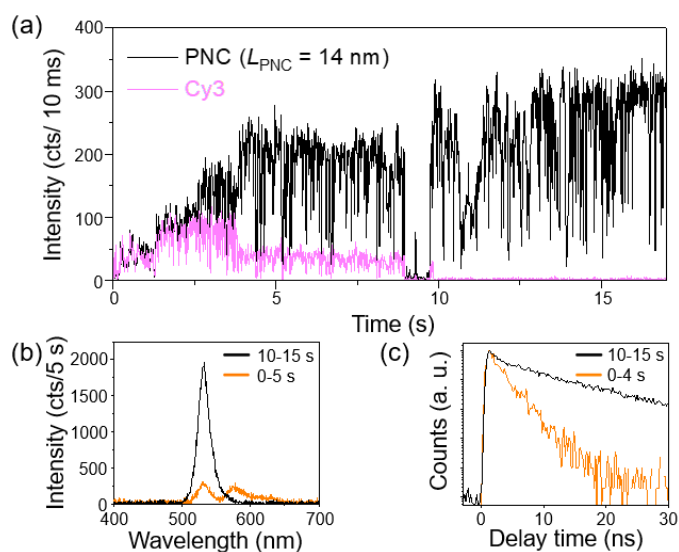


Figure S35. (a) Time traces of PL intensity detected from Cy3 (pink line) and the PNC (black line) in a single **PNC-Cy3** system under 442 nm excitation. (b) PL spectra collected from the single **PNC-Cy3** system during 0–5 s (orange line) and 10–15 s (black line) in the time trace shown in (a). The PNC size was estimated to be $L_{\text{PNC}} = 14$ nm based on the PL peak. (c) PL decay curves of the PNC detected during 0–4 s (orange line) and 10–15 s (black line) in the time trace shown in (a).

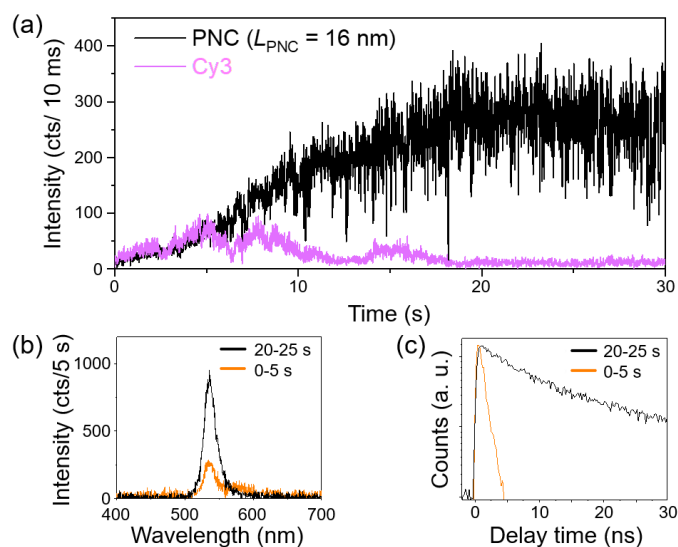


Figure S36. (a) Time traces of PL intensity detected from Cy3 (pink line) and the PNC (black line) in a single **PNC-Cy3** system under 442 nm excitation. (b) PL spectra collected from the single **PNC-Cy3** system during 0–5 s (orange line) and 20–25 s (black line) in the time trace shown in (a). The PNC size was estimated to be $L_{\text{PNC}} = 16$ nm based on the PL peak. (c) PL decay curves of the PNC detected during 0–5 s (orange line) and 20–25 s (black line) in the time trace shown in (a).

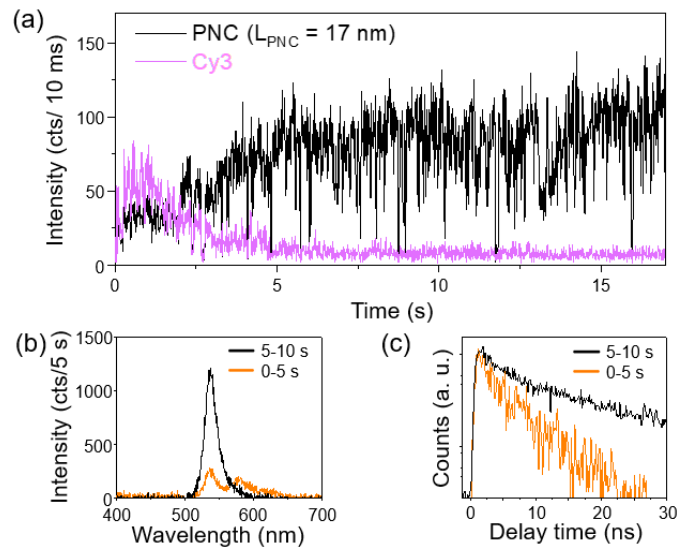


Figure S37. (a) Time traces of PL intensity detected from Cy3 (pink line) and the PNC (black line) in a single **PNC-Cy3** system under 442 nm excitation. (b) PL spectra collected from the single **PNC-Cy3** system during 0–5 s (orange line) and 5–10 s (black line) in the time trace shown in (a). The PNC size was estimated to be $L_{\text{PNC}} = 17$ nm based on the PL peak. (c) PL decay curves of the PNC detected during 0–5 s (orange line) and 5–10 s (black line) in the time trace shown in (a).

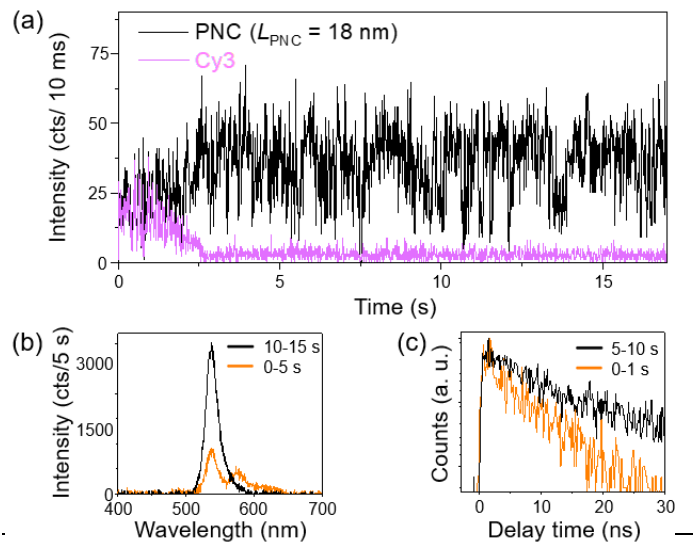


Figure S38. (a) Time traces of PL intensity detected from Cy3 (pink line) and the PNC (black line) in a single **PNC-Cy3** system under 442 nm excitation. (b) PL spectra collected from the single **PNC-Cy3** system during 0–5 s (orange line) and 10–15 s (black line) in the time trace shown in (a). The PNC size was estimated to be $L_{\text{PNC}} = 17$ nm based on the LP peak. (c) PL decay curves of the PNC detected during 0–1 s (orange line) and 5–10 s (black line) in the time trace shown in (a).

12. Evaluation of ET from MX in a single PNC to multiple Cy3 dyes

To evaluate ET from MX in the PNCs to multiple Cy3 adsorbed on the PNC surfaces, PL photon statistics of Cy3 in the **PNC-Cy3** systems were analyzed at the single **PNC-Cy3** level by 442 nm excitation. The PL from Cy3, resulting from FRET from the PNCs, was detected by two APDs through an LP filter. Time traces of PL intensity, PL spectra, and photon correlation histograms obtained from individual **sPNC-Cy3**, **mPNC-Cy3**, and **L_{PNC}-Cy3** are shown in Figures S39-S50.

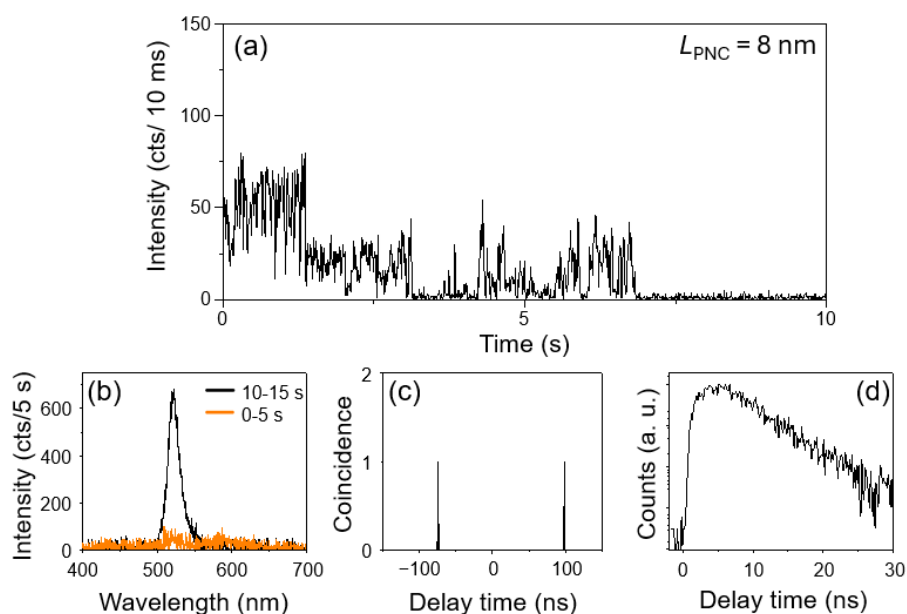


Figure S39. Time trace of PL intensity (a), PL spectra detected between 0–5 s (orange line) and 10–15 s (black line) in the time trace (b), photon correlation histogram (c), and PL decay curve (d) detected from Cy3 in a single **PNC-Cy3** by exciting at 442 nm. The PNC size was estimated to be $L_{\text{PNC}} = 8 \text{ nm}$ based on the PL peak.

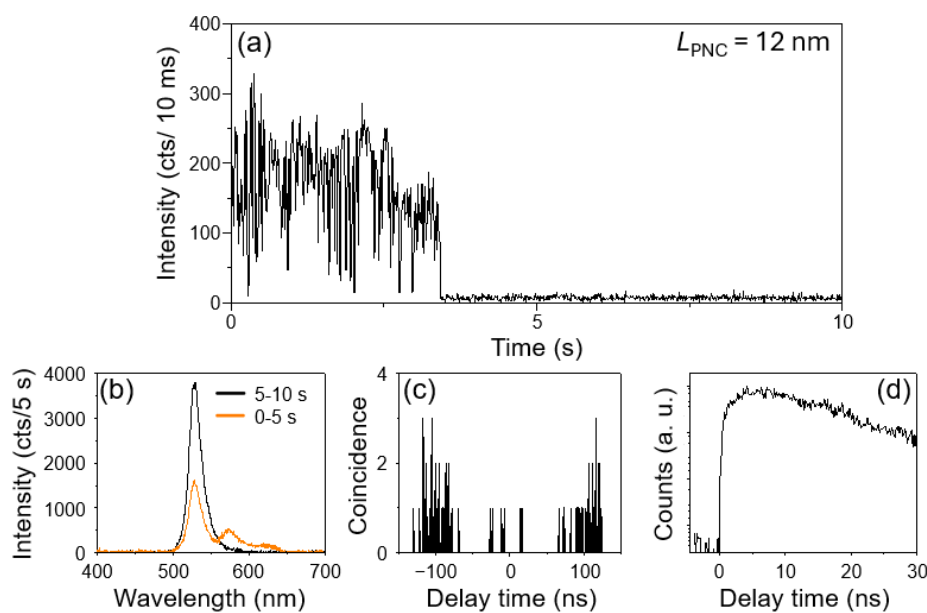


Figure S40. Time trace of PL intensity (a), PL spectra detected between 0–5 s (orange line) and 5–10 s (black line) in the time trace (b), photon correlation histogram (c), and PL decay curve (d) detected from Cy3 in a single **PNC-Cy3** by exciting at 442 nm. The PNC size was estimated to be $L_{\text{PNC}} = 12$ nm based on the PL peak.

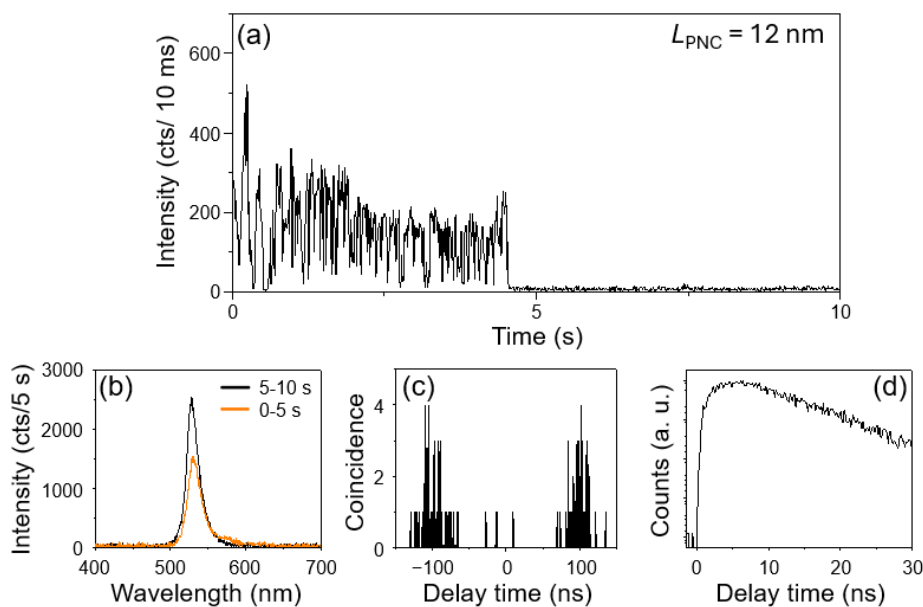


Figure S41. Time trace of PL intensity (a), PL spectra detected between 0–5 s (orange line) and 5–10 s (black line) in the time trace (b), photon correlation histogram (c), and PL decay curve (d) detected from Cy3 in a single **PNC-Cy3** by exciting at 442 nm. The PNC size was estimated to be $L_{\text{PNC}} = 12$ nm based on the PL peak.

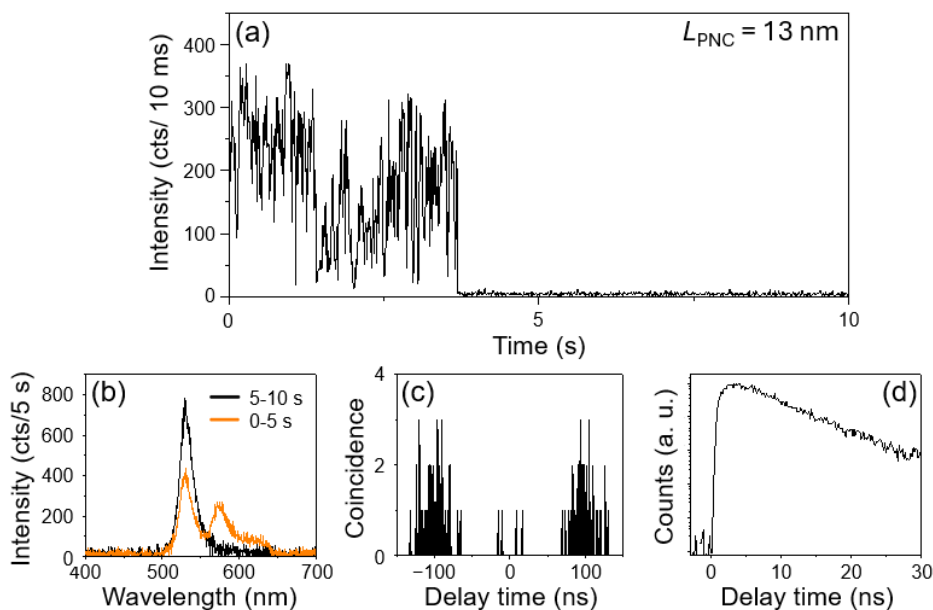


Figure S42. Time trace of PL intensity (a), PL spectra detected between 0–5 s (orange line) and 10–15 s (black line) in the time trace (b), photon correlation histogram (c), and PL decay curve (d) detected from Cy3 in a single **PNC-Cy3** by exciting at 442 nm. The PNC size was estimated to be $L_{\text{PNC}} = 13$ nm based on the PL peak.

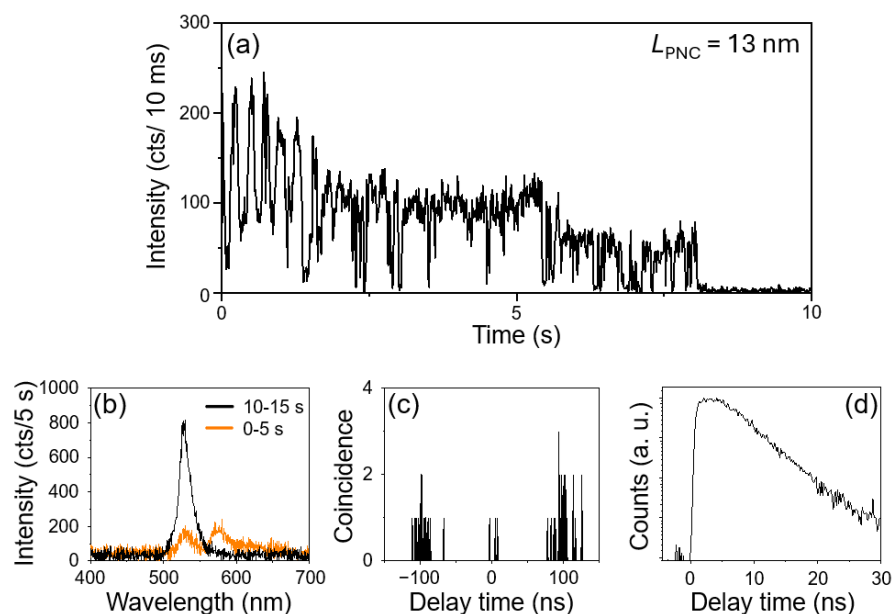


Figure S43. Time trace of PL intensity (a), PL spectra detected between 0–5 s (orange line) and 10–15 s (black line) in the time trace (b), photon correlation histogram (c), and PL decay curve (d) detected from Cy3 in a single **PNC-Cy3** by exciting at 442 nm. The PNC size was estimated to be $L_{\text{PNC}} = 13$ nm based on the PL peak.

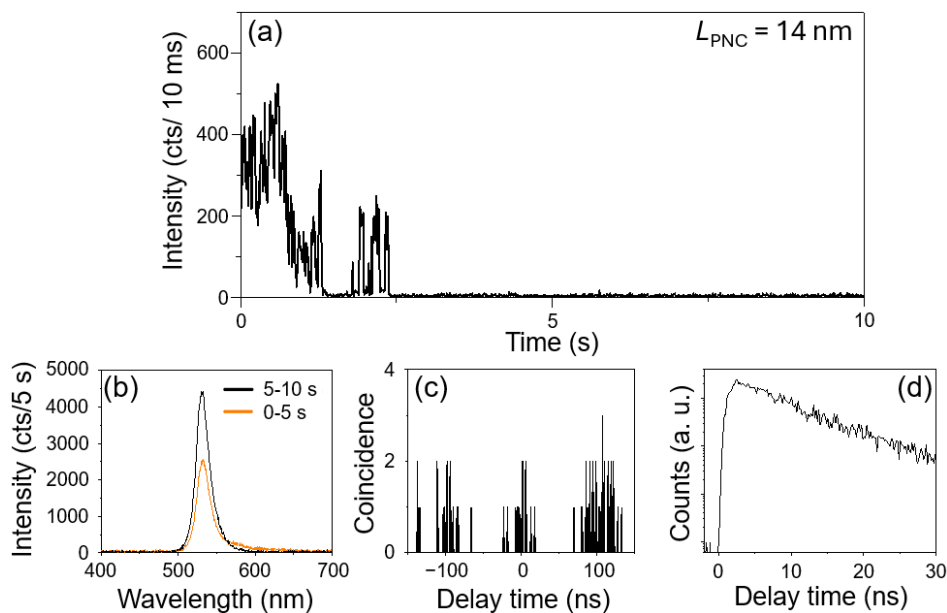


Figure S44. Time trace of PL intensity (a), PL spectra detected between 0–5 s (orange line) and 5–10 s (black line) in the time trace (b), photon correlation histogram (c), and PL decay curve (d) detected from Cy3 in a single **PNC-Cy3** by exciting at 442 nm. The PNC size was estimated to be $L_{\text{PNC}} = 14 \text{ nm}$ based on the PL peak.

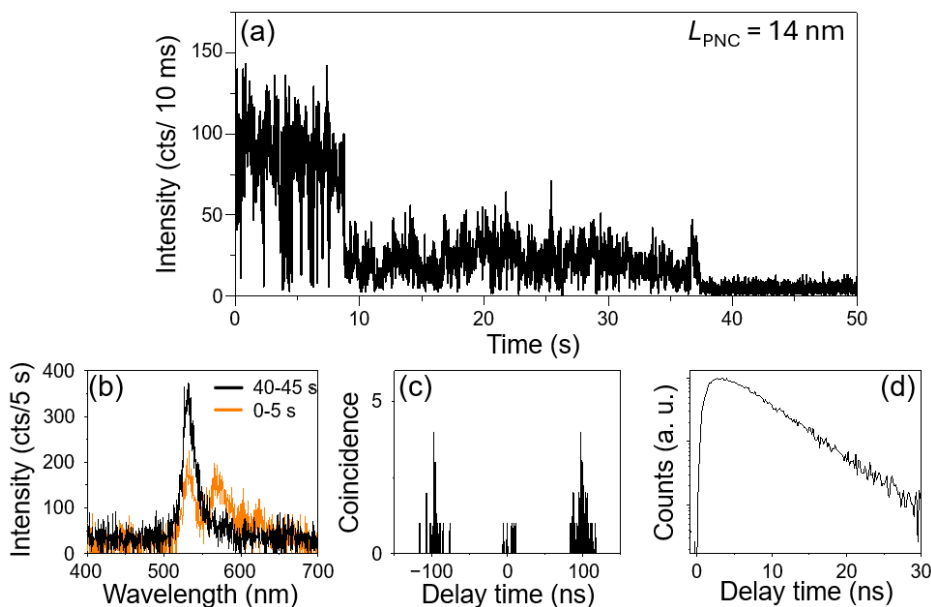


Figure S45. Time trace of PL intensity (a), PL spectra detected between 0–5 s (orange line) and 40–45 s (black line) in the time trace (b), photon correlation histogram (c), and PL decay curve (d) detected from Cy3 in a single **PNC-Cy3** by exciting at 442 nm. The PNC size was estimated to be $L_{\text{PNC}} = 14 \text{ nm}$ based on the PL peak.

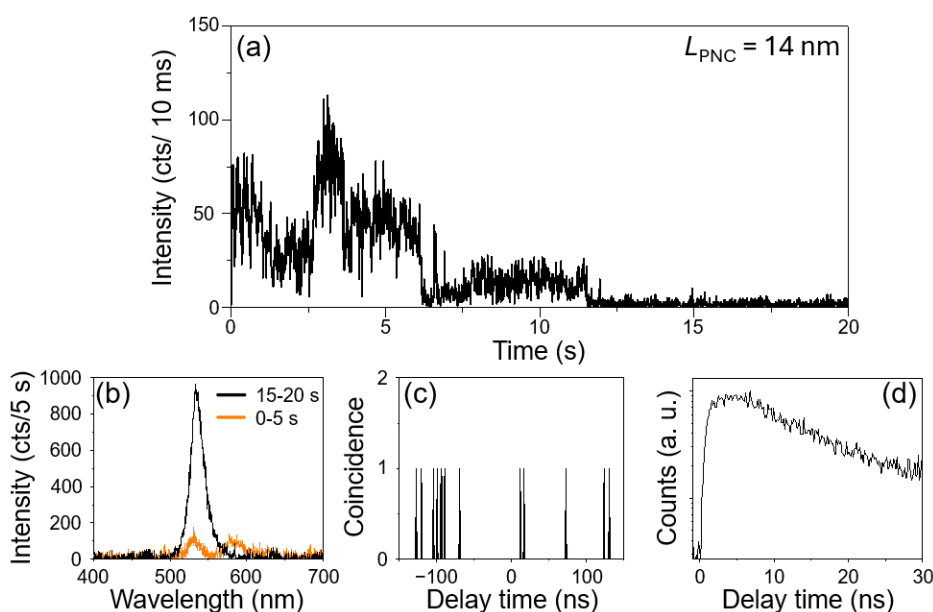


Figure S46. Time trace of PL intensity (a), PL spectra detected between 0–5 s (orange line) and 15–20 s (black line) in the time trace (b), photon correlation histogram (c), and PL decay curve (d) detected from Cy3 in a single **PNC-Cy3** by exciting at 442 nm. The PNC size was estimated to be $L_{\text{PNC}} = 14$ nm based on the PL peak.

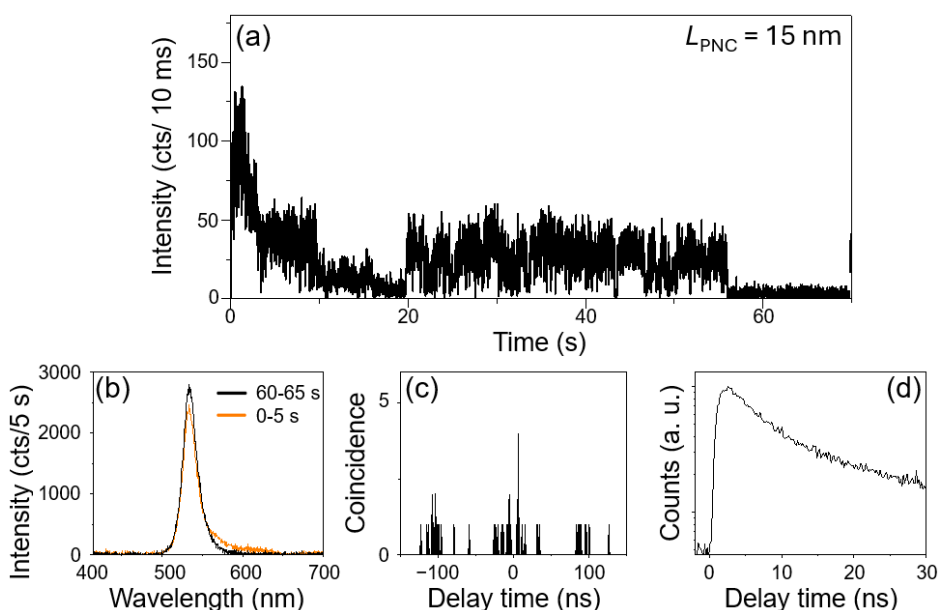


Figure S47. Time trace of PL intensity (a), PL spectra detected between 0–5 s (orange line) and 60–65 s (black line) in the time trace (b), photon correlation histogram (c), and PL decay curve (d) detected from Cy3 in a single **PNC-Cy3** by exciting at 442 nm. The PNC size was estimated to be $L_{\text{PNC}} = 15$ nm based on the PL peak.

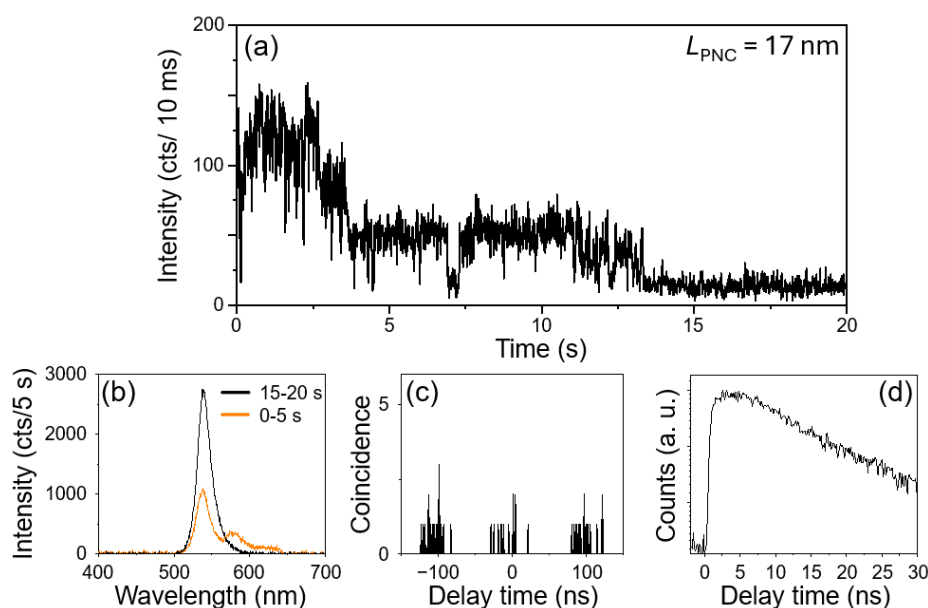


Figure S48. Time trace of PL intensity (a), PL spectra detected between 0–5 s (orange line) and 15–20 s (black line) in the time trace (b), photon correlation histogram (c), and PL decay curve (d) detected from Cy3 in a single **PNC-Cy3** by exciting at 442 nm. The PNC size was estimated to be $L_{\text{PNC}} = 17$ nm based on the PL peak.

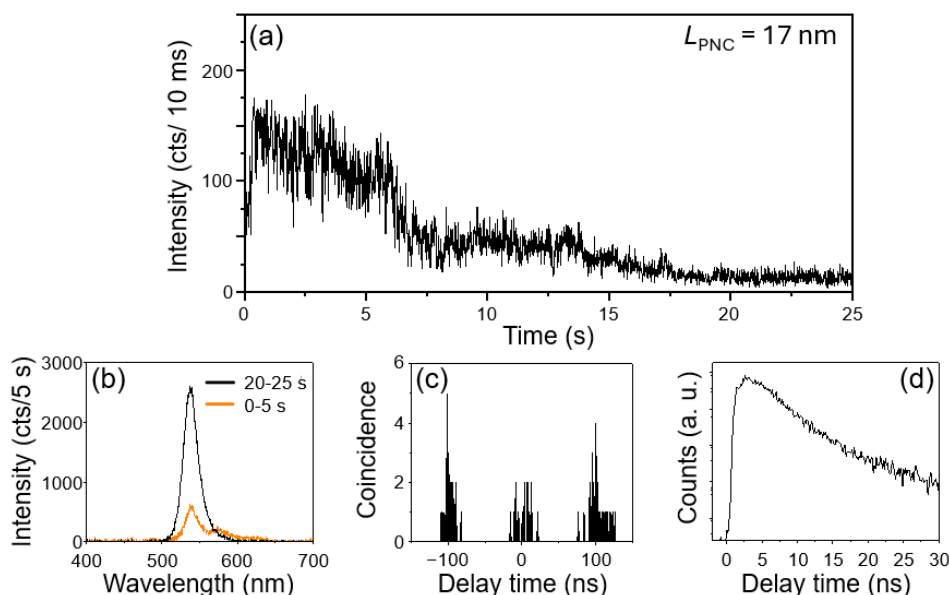


Figure S49. Time trace of PL intensity (a), PL spectra detected between 0–5 s (orange line) and 20–25 s (black line) in the time trace (b), photon correlation histogram (c), and PL decay curve (d) detected from Cy3 in a single **PNC-Cy3** by exciting at 442 nm. The PNC size was estimated to be $L_{\text{PNC}} = 17$ nm based on the PL peak.

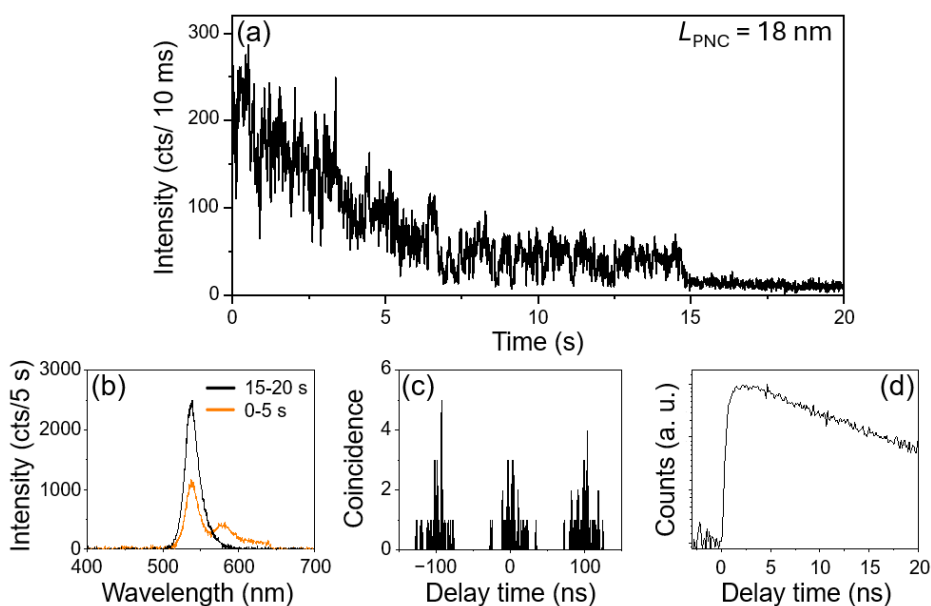


Figure S50. Time trace of PL intensity (a), PL spectra detected between 0–5 s (orange line) and 15–20 s (black line) in the time trace (b), photon correlation histogram (c), and PL decay curve (d) detected from Cy3 in a single **PNC-Cy3** by exciting at 442 nm. The PNC size was estimated to be $L_{\text{PNC}} = 18 \text{ nm}$ based on the PL peak.

REFERENCES

- (1) Yarita, N.; Tahara, H.; Saruyama, M.; Kawawaki, T.; Sato, R.; Teranishi, T.; Kanemitsu, Y. Impact of Postsynthetic Surface Modification on Photoluminescence Intermittency in Formamidinium Lead Bromide Perovskite Nanocrystals. *J. Phys. Chem. Lett.* **2017**, *8* (24), 6041-6047. DOI: 10.1021/acs.jpcclett.7b02840.
- (2) Maes, J.; Balcaen, L.; Drijvers, E.; Zhao, Q.; De Roo, J.; Vantomme, A.; Vanhaecke, F.; Geiregat, P.; Hens, Z. Light Absorption Coefficient of CsPbBr₃ Perovskite Nanocrystals. *J. Phys. Chem. Lett.* **2018**, *9* (11), 3093-3097. DOI: 10.1021/acs.jpcclett.8b01065.
- (3) Ishibashi, Y.; Arinishi, M.; Katayama, T.; Miyasaka, H.; Asahi, T. Femtosecond excited-state dynamics of fullerene-C(60) nanoparticles in water. *Phys. Chem. Chem. Phys.* **2018**, *20* (2), 958-966. DOI: 10.1039/c7cp06746a.
- (4) Steinberg, I. Z. Long-Range Nonradiative Transfer of Electronic Excitation Energy in Proteins and Polypeptides. *Annu. Rev. Biochem.* **1971**, *40*, 83-114. DOI: 10.1146/annurev.bi.40.070171.000503.
- (5) Yamamoto, M.; Morimoto, M.; Irie, M.; Eguchi, D.; Tamai, N. Deciphering the

Optical Switching Mechanism of CdSe/CdS QDs Luminescence by Diarylethene Molecular Photoswitches: A Stochastic Model Analysis. *J. Phys. Chem. C* **2024**, *128* (46), 19758-19766. DOI: 10.1021/acs.jpcc.4c06245.